Veterinary Research

RESEARCH ARTICLE

Open Access

Integrated transcriptomic and metabolomic analysis identifies host response mechanisms to oncogenic Marek's disease virus in Wenchang chickens

Xiangdong Xu[1,2†], Junming Zhao[3†], Sanchun He[2], Yuting Fang[2], Dan Liu[2], Tingbo Shen[2], Lifeng Zhi[2], Zheng Liu[4], Liguang Shi[1], Guanyu Hou[1], Runfeng Zhang[2*] and Guang Rong[1*]

Abstract

Marek's disease (MD), caused by Marek's disease virus (MDV), poses a significant threat to the poultry industry worldwide by inducing neurological disorders and malignant lymphoma in infected chickens. The underlying mechanisms of the host response to MDV infection and tumorigenesis remain poorly understood. To gain insight into the host response, we analysed the transcriptomic and metabolomic profiles of the heart tissue of Wenchang chickens, an indigenous Chinese breed, using RNA sequencing and untargeted metabolomics. A total of 2470 and 2666 genes were significantly up- and down-regulated, respectively, between infected and uninfected chickens. KEGG pathway enrichment analysis revealed distinct transcriptional patterns in response to MDV infection: upregulated genes were enriched primarily in immunity-related pathways, whereas downregulated genes were associated with metabolic pathways. Among the 433 differentially expressed metabolites identified, only the caffeine metabolism pathway approached statistical significance ($p = 0.067$). Integrative mapping of genes and metabolites to the KEGG enzyme database highlighted L-tryptophan interactions, with KYNU, KMO, KYAT3, and AADAT as the most representative relationships. These results provide a quantitative overview of MDV-induced transcriptional and metabolic perturbations, suggesting that hosts may counteract viral infection and tumor progression by suppressing cellular metabolism to potentiate immune responses.

Keywords Marek's disease, host response, transcriptomics, metabolomics, chicken

Handling editor: Kate Sutton

†Xiangdong Xu and Junming Zhao contributed equally to this work.

*Correspondence:
Runfeng Zhang
zrfeng163@126.com
Guang Rong
rongguangxn@163.com
[1] Tropical Crops Genetic Resources Institute, Chinese Academy of Tropical Agricultural Sciences, Hainan Province, Haikou, China
[2] Huangshi Biomedicine Industry and Technology Research Institute, Hubei Key Laboratory of Edible Wild Plants Conservation and Utilization, College of Life Sciences, Hubei Normal University, Huangshi, Hubei Province, China
[3] Key Lab of Tropical Crops Information Technology Application Research of Hainan Province, Institute of Science and Technology Information, Chinese Academy of Tropical Agricultural Sciences, Haikou, Hainan Province, China
[4] Agriculture and Rural Affairs Bureau of Yangxin County, Huangshi, Hubei Province, China

© The Author(s) 2025. **Open Access** This article is licensed under a Creative Commons Attribution 4.0 International License, which permits use, sharing, adaptation, distribution and reproduction in any medium or format, as long as you give appropriate credit to the original author(s) and the source, provide a link to the Creative Commons licence, and indicate if changes were made. The images or other third party material in this article are included in the article's Creative Commons licence, unless indicated otherwise in a credit line to the material. If material is not included in the article's Creative Commons licence and your intended use is not permitted by statutory regulation or exceeds the permitted use, you will need to obtain permission directly from the copyright holder. To view a copy of this licence, visit http://creativecommons.org/licenses/by/4.0/. The Creative Commons Public Domain Dedication waiver (http://creativecommons.org/publicdomain/zero/1.0/) applies to the data made available in this article, unless otherwise stated in a credit line to the data.

Introduction

Marek's disease (MD) is a major health problem in poultry production systems worldwide and causes an annual global economic loss of approximately $2 billion [1]. MD is a complex immunosuppressive and lymphoproliferative disease of chickens. The pathological features of MD include paralysis, neuroinflammation, and chronic depletion, as well as visceral and muscle lymphomas in chickens [2–4]. The causal agent is a naturally occurring α-herpesvirus with double-stranded DNA called Gallid alphaherpesvirus 2 (GaHV2), commonly referred to as Marek's disease herpesvirus (MDV). MDV toxicity progresses from mildly virulent (m), virulent (v), and very virulent (vv) to very virulent plus (vv+) [5]. Invasion by virulent and very virulent strains causes transient paralysis in most breeds, and very virulent plus strains cause brain damage and eventually death [6]. Moreover, as the virus evolves, the virulence of MDV gradually increases [5]. In the "Cornell model" [7], MDV undergoes a long and complex pathogenic life cycle involving four phases: (a) the early cytolytic phase (2–7 days post-infection (dpi)), (b) the latent phase (from 7 to 10 dpi), (c) the late cytolytic and immunosuppressive phase (from 18 dpi) and (d) the proliferative phase (from 28 dpi).

MDV infection induces a complex process that activates various components of the host immune system along with virus-induced physiological changes and ultimately leads to lymphoid tumours in susceptible chickens. Considerable efforts have been made in recent years to investigate the basis of host immune responses to MDV infection, with a focus on the experimental White Leghorn (layer) lines 6_3 and 7_2, which are MD resistant and susceptible, respectively. Genome-wide QTL mapping studies have identified loci or domains associated with MD resistance or susceptibility on chromosomes 1, 5, 7, 9, 15, 18, 26, Z, E21, and E16 [8–14]. Available chicken microarrays have become useful tools to study the gene and protein expression profiles of MDV-host interactions and to further elucidate the molecular mechanisms involved in pathogenic and tumorigenic responses to MDV infection. Genome-wide microarray analyses revealed genes with dysregulated expression in response to MDV exposure in embryonic fibroblasts, peripheral blood leukocytes, lymph nodes, or chicken epithelial tissues [13, 15–21]. These candidate genes are involved in many biological processes involved in host–pathogen interactions, such as antigen presentation, the interferon (IFN) response, signal transduction, the cytoskeleton, the immune response, cell surface molecules, and apoptosis. Recently, several studies have employed RNA sequencing technology coupled with quantitative real-time PCR to explore the dynamic and differential gene expression profiles of the liver, thymus, spleen, or bursa of Fabricius of MDV-infected chickens [22–25] and revealed more than 5000 genes with dysregulated expression at different stages upon induction of MDV exposure.

MDV uses and reshapes the metabolic network of the host to facilitate its own replication and assembly. MDV infection can increase arginase activity in macrophages, altering the metabolism of various amino acids, including arginine, which play a key role in promoting tumorigenesis [26]. Moreover, MDV infection can regulate the metabolic reprogramming of host cell glycolysis by increasing the activity of mitochondrial fatty acid β-oxidation, which can increase the oxygen consumption rate in MDV-infected cells, ultimately leading to an increase in glycolysis to promote virus replication [27]. MDV infection can significantly alter metabolites in chicken embryo fibroblasts, with most changes occurring in amino acid metabolism, energy metabolism, nucleotide metabolism, and lipid metabolism, especially the upregulation of amino acids in host cells during the early stages of infection to provide the energy and intermediary metabolites necessary for efficient multiplication of its own replication [28]. The modification of metabolic signalling pathways in host cells during the infection process is evident, which may have a significant impact on the pathogenesis of MDV.

Although these studies have expanded our understanding of MDV infection, the molecular mechanisms of host–virus interactions in MD are far from fully understood. Further studies are necessary to elucidate the exact mechanisms by which the host responds to virus infection in terms of immunity and metabolism, thereby providing deeper insight into this fascinating biological phenomenon. In this study, we employed RNA sequencing (RNA-seq) and an untargeted metabolic approach to discern transcriptomic and metabolomic changes in chickens naturally infected with MDV. Our findings demonstrated that many genes and metabolites are significantly altered during MDV infection. These alterations suggest potential molecular mechanisms of the host immune response along with MD pathogenesis and tumorigenesis.

Materials and methods

Animals and sample collection

The broiler Wenchang birds hatched in the same batch were kept and managed in two separate houses under the same conditions at the farming base of Yexiang Wenchang Chicken Breeding Co., Ltd., in Hainan Province. At 60 days of age, 30% of the birds presented classic clinical signs of Marek's disease, including lethargy, glazed eyes, paralysis, anorexia, and pathological emaciation. Symptomatic chickens were immediately transferred to isolated houses, and asymptomatic chickens remained

in the original facility. At 70 days of age, five chickens that exhibited clinical symptoms and five asymptomatic chickens were humanely euthanized via CO_2 asphyxiation (30% chamber volume/min) followed by confirmatory cervical dislocation. Three subsamples from the same heart tissue were taken for MDV detection, RNA-seq and metabolomic analysis and quickly frozen in liquid nitrogen for further use. At the same time, anticoagulant blood samples were collected for detection of avian leukosis virus (ALV). The animal experiments were approved by the Animal Care and Use Committee of the Chinese Academy of Tropical Agricultural Sciences and were conducted in accordance with the Guidelines for Experimental Animals of the Ministry of Science and Technology (Beijing, China).

Viral infection detection

ELISA and PCR were performed to detect ALV and/or MDV infection in these two groups according to the Chinese ALV disease diagnostic methods and the Chinese Marek's disease diagnostic methods (GT/B 26436-2010 and GBT18643-2021), respectively.

Transcriptomic analysis and quantitative real-time polymerase chain reaction (qRT–PCR)

Total RNA from frozen heart tissues was extracted using TRIzol reagent (Invitrogen, Carlsbad, CA, USA) following the manufacturer's instructions. The RNA content of each sample was then determined using a NanoDrop One (Thermo Fisher Scientific, MA, USA). The quality of the RNAs was then determined using an Agilent 2100 Bioanalyzer (Agilent Technologies, Santa Clara, CA, USA), and RNA integrity was measured by denatured agarose gel electrophoresis. The extracted RNA was then prepared using the NEBNext Ultra Directional RNA Library Prep Kit (New England Biolabs, Ipswich, MA, USA). Libraries were subjected to 150 bp paired-end sequencing on an Illumina HiSeq2000 sequencer.

Clean reads were obtained from raw sequencing reads after removing sequencing adaptors, duplicated sequences, and low-quality reads and then mapped against the chicken reference genome Gallus_gallus. GRCg6a (version 105.6) was generated via HISAT2 (v2.0.5) with the default parameters [29]. The uniquely mapped reads were counted to calculate the number of reads per gene using HTSeq (2.0.2) [30]. Differentially expressed genes (DEGs) were identified between the infected and uninfected groups using DESeq2 [31] and then filtered with a false discovery rate (FDR) ≤ 0.05 and $|\log_2 \text{FoldChange}| \geq 1$. To better understand the functional involvement of these DEGs, topGO [32] and clusterProfiler [33] were used for GO and KEGG pathway enrichment analysis. The DEG network was developed using NetworkAnalyst [34], which is based on protein–protein interactions derived from SRTING (Interacting Genes/Proteins, version 11.5).

Ten genes were chosen to validate the results obtained from the RNA-seq analysis by qRT-PCR (Additional file 1). Complementary DNA (cDNA) was synthesized from total RNA using HiScript® Q RT SuperMix for qPCR (+gDNA wiper) (Vazyme, Nanjing, China) according to the manufacturer's instructions. All PCR reactions were carried out in a QuantStudio™ 5 Real-Time PCR System (Applied Biosystems, USA). The reactions were run in triplicate in a total volume of 10 µL containing the following: 2.0 µL of cDNA (100 ng), 0.25 µL of each primer (forward and reverse, 10 nM each), 5.0 µL of 2×ChamQ SYBR qPCR Master Mix (Vazyme, Nanjing, China) and 2.5 µL of nuclease-free water. The amplification reactions were subjected to initial denaturation at 95 ℃ for 30 s, followed by 40 cycles of denaturation at 95 ℃ for 10 s, annealing at 60 ℃ for 30 s, and 72 ℃ for 20 s. The relative gene expression of each target gene was calculated using the $2^{-\Delta\Delta Ct}$ method with glyceraldehyde-3-phosphate dehydrogenase (GAPDH) as the internal reference.

Metabolomic analysis

Flesh samples were thawed at 4 ℃ and homogenized using a grinding pestle. A 100 µL aliquot of the homogenized sample was transferred into a 2 mL centrifuge tube containing 1000 µL of methanol, followed by grinding for 1 min. The sample was then centrifuged at 12,000 rpm for 10 min at 4 °C. The supernatant was transferred to a new 2 mL centrifuge tube and concentrated until drying. The residue was reconstituted in 200 µL of 2-chloro-L-phenylalanine (4 ppm) solution prepared in 80% methanol water (stored at 4 ℃), filtered through a 0.22 µm membrane, and transferred to a detection bottle for liquid chromatography–tandem mass spectrometry (LC–MS) analysis.

Metabolite analysis of the heart tissues was conducted by PANOMIX (Suzhou, China) using an LC–MS system comprising a Vanquish UHPLC System and Orbitrap Exploris 120 mass spectrometer (Thermo Fisher Scientific, USA). The extracts were injected onto an ACQUITY UPLC® HSS T3 column (2.1×100 mm, 1.8 µm, Waters, Milford, MA, USA), which was maintained at 40 °C. The temperature, flow rate and injection volume of the automatic injector were set at 4 °C, 0.3 mL/min and 2 µL, respectively [35]. Mass spectrometric detection of metabolites was performed on an Orbitrap Exploris 120 (Thermo Fisher Scientific, USA) with an ESI ion source [36]. Simultaneous MS1 and MS/MS (full MS–ddMS2 mode, data-dependent MS/MS) acquisition was used. Metabolite identification was performed with high

precision, initiated by accurate m/z measurements followed by MS/MS fragmentation pattern analysis. Cross-referencing of the identified metabolites was performed against the Human Metabolome Database (HMDB), MassBank, LipidMaps, mzCloud, and the metabolite database built by PANOMIX (Shuzhou, China) to confirm and validate the findings. Two different multivariate statistical analysis models, unsupervised and supervised, were applied to discriminate the groups (PCA; PLS-DA; OPLS-DA) by Ropls (v1.22.0) package [37]. Differentially expressed metabolites (DEMs) were selected (VIP > 1 and p value < 0.05). KEGG and MetaboAnalyst [38] were used to search for metabolite pathways.

Transcriptome and metabolome association analysis

The associations between DEGs and DEMs were analysed on the basis of the Pearson correlation coefficient. All DEGs and metabolites were mapped to the KEGG pathway database, and their common pathway information was obtained. The main biochemical and signal transduction pathways were subsequently analysed. The networks of genes and metabolites were analysed by igraph software [39].

Results

Viral infection identification

ELISA of the ALV p27 antigen revealed that the OD values of all the samples were less than 0.2 (the OD value for the negative control was less than 0.2, and that for the positive control was greater than 0.8) after the DF-1 cells were infected with the viral mixture and cultured for 7 days. These results indicate that these individuals are negative for ALV infection.

The PCR results revealed that a specific fragment of 786 bp for the MDV *meq* gene and a specific fragment of 317 bp for MDV 132 *bpr* were amplified from samples of sick birds, whereas neither of the two fragments were amplified from samples of healthy birds, confirming that those sick birds were infected by MDV (Additional file 2).

Transcriptomic analysis

Ten cDNA libraries were constructed for the hearts of infected and uninfected chickens, resulting in 60.39 GB of clean reads, including 400 004 580 reads after quality control assessment. Approximately 97.68% of the raw reads (± 2.96%, SD) were uniquely mapped to the chicken genome assembly. A total of 5,136 DEGs were identified between the infected and uninfected groups (FDR ≤ 0.05 and $|\log_2\text{FoldChange}| \geq 1$). Compared with the uninfected group, the infected group presented 2470 and 2666 up- and down-regulated genes, respectively (Figure 1A, Additional file 3). All DEGs were mapped to KEGG pathways, and 19 significantly enriched pathways were obtained (Figure 1B, Additional file 4), among which Salmonella infection, cytokine–cytokine receptor interaction, focal adhesion, oxidative phosphorylation, and the NOD-like receptor signalling pathway were the five most representative pathways. The upregulated DEGs were significantly enriched in 24 pathways related mainly to the immune system, cell growth and death, and infectious diseases, including the Toll-like receptor signalling pathway, NOD-like receptor signalling pathway, apoptosis, lysosome, herpes simplex virus 1 infection, and influenza A (Figure 1B). The downregulated DEGs were mostly related to carbohydrate metabolism, the circulatory system and amino acid metabolism, as shown by enriched KEGG pathways such as oxidative phosphorylation; valine, leucine and isoleucine degradation; myocardial contraction; the citrate cycle (TCA cycle); and propanoate metabolism (Figure 1B).

The RNA-seq results of selected genes were validated in the same sample set by qRT–PCR (Figure 1C). The correlation coefficient (R) of the $\log_2$-transformed fold change values between the qRT–PCR and RNA–seq platforms was 0.952 (Figure 1D). The expression results of ALPK2, APLNR, ATP6V0D2, CA8, CKMT2, CYBB, IL22RA2, MMP9, SLC6A4, and STEAP4 obtained by qRT–PCR were in good agreement with the RNA–seq results ($p < 0.001$).

Metabolomic analysis

Multivariate statistical analysis revealed a clear separation of metabolites between the infected and noninfected groups in the negative model (Figure 2A) and the cation model (Figure 2B). A total of 433 DEMs (261 negative model and 172 positive model) were identified by setting thresholds of VIP > 1 and p value < 0.05, including 372 upregulated and 61 downregulated DEMs (Figure 2C, Additional file 5). Among these DEMs, dihydroxyfumitremorgin C ($\log_2\text{FoldChange} = 6.7$) and L-kynurenine ($\log_2\text{FoldChange} = 6.64$) presented the greatest increases in the positive and negative models, respectively, whereas pantetheine 4'-phosphate ($\log_2\text{FoldChange} = -4.52$) and 2-biphenylol ($\log_2\text{FoldChange} = -6.46$) presented the lowest decreases in infected birds. All the DEMs were subjected to KEGG annotation analysis, and only the caffeine metabolism pathway was nearly significantly enriched ($p = 0.067$) (Figure 2D, Additional file 6).

Comprehensive analysis of transcriptomics and metabolomics

Through Pearson correlation analysis, correlations between differentially expressed genes (DEGs) from transcriptomics and differentially expressed metabolites (DEMs) from metabolomics were calculated. Correlation coefficients greater than 0 indicated positive

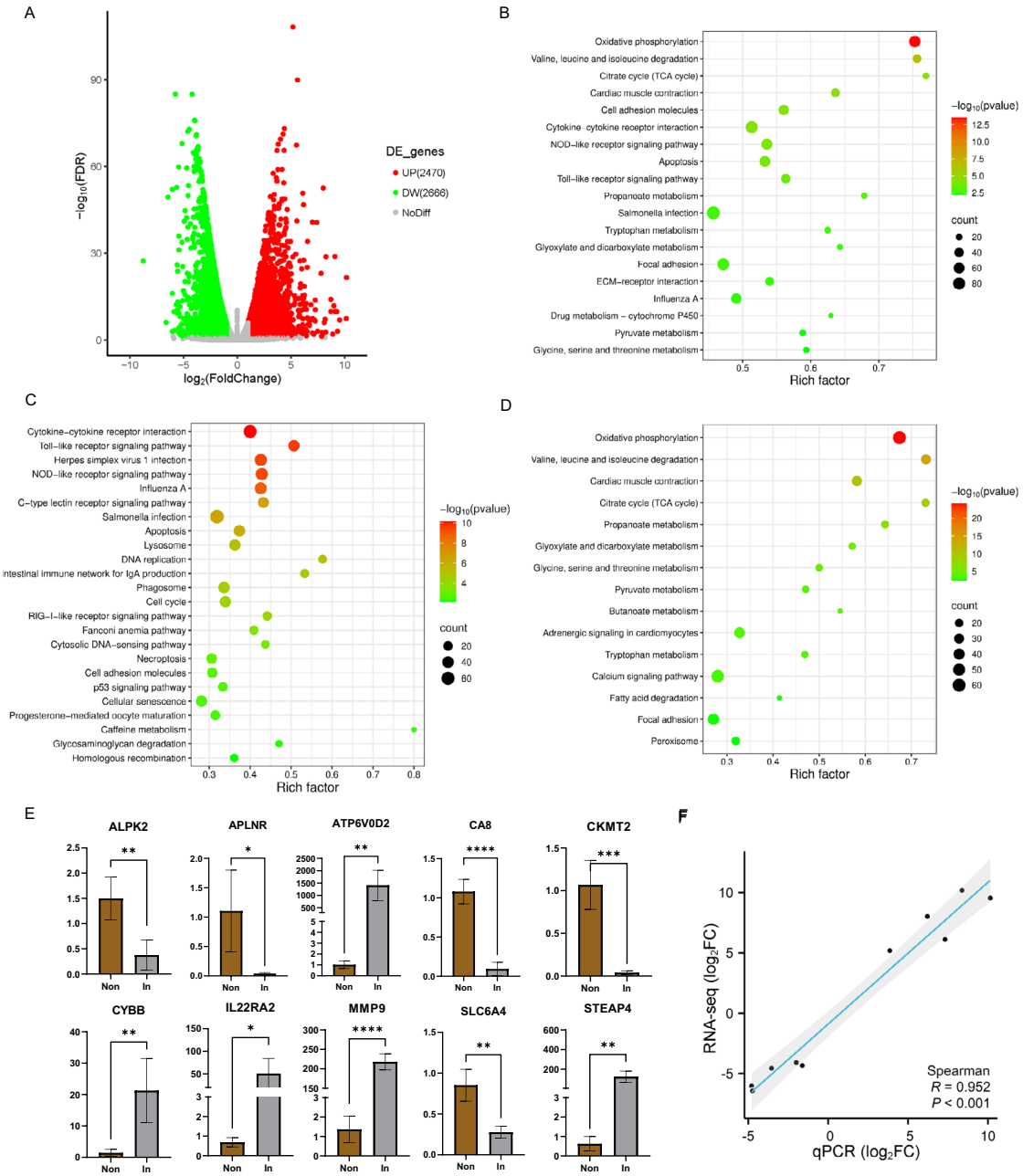

Figure 1 Transcriptomic pattern variation in the heart tissues of Wenchang chickens infected with MDV. **A** Volcano plot. The red and green colours indicate genes detected as up- and down-regulated in the infected group compared with the uninfected group at FDR < 0.05. **B** Bubble plots for KEGG pathways enrichment of DEGs. **C** Bubble plots for KEGG pathways enrichment of upregulated DEGs. **D** Bubble plots for KEGG pathways enrichment of downregulated DEGs. **E** Real-Time RT-PCR analysis of selected genes. Relative expression levels calculated from standard curves were normalized to the endogenous control GAPDH gene. Numbers represent mean plus standard error. ALPK2: alpha kinase 2; APLNR: apelin receptor; ATP6V0D2: ATPase H + transporting V0 subunit d2; CA8: carbonic anhydrase 8; CKMT2: creatine kinase, mitochondrial 2; CYBB: cytochrome b-245 beta chain; IL22RA2: interleukin 22 receptor subunit alpha 2; MMP9: matrix metalloproteinase 9; SLC6A4: solute carrier family 6 member 4; STEAP4: Six-transmembrane epithelial antigen of the prostate 4. *$p < 0.05$; **$p < 0.01$. **F** Correlation of fold changes calculated from qPCR and RNAseq analysis. Black dots represent $\log_2$ transformed fold change values of a single gene in an infected sample obtained from qPCR (X-axis) and RNAseq analysis (Y-axis). R: correlation coefficient.

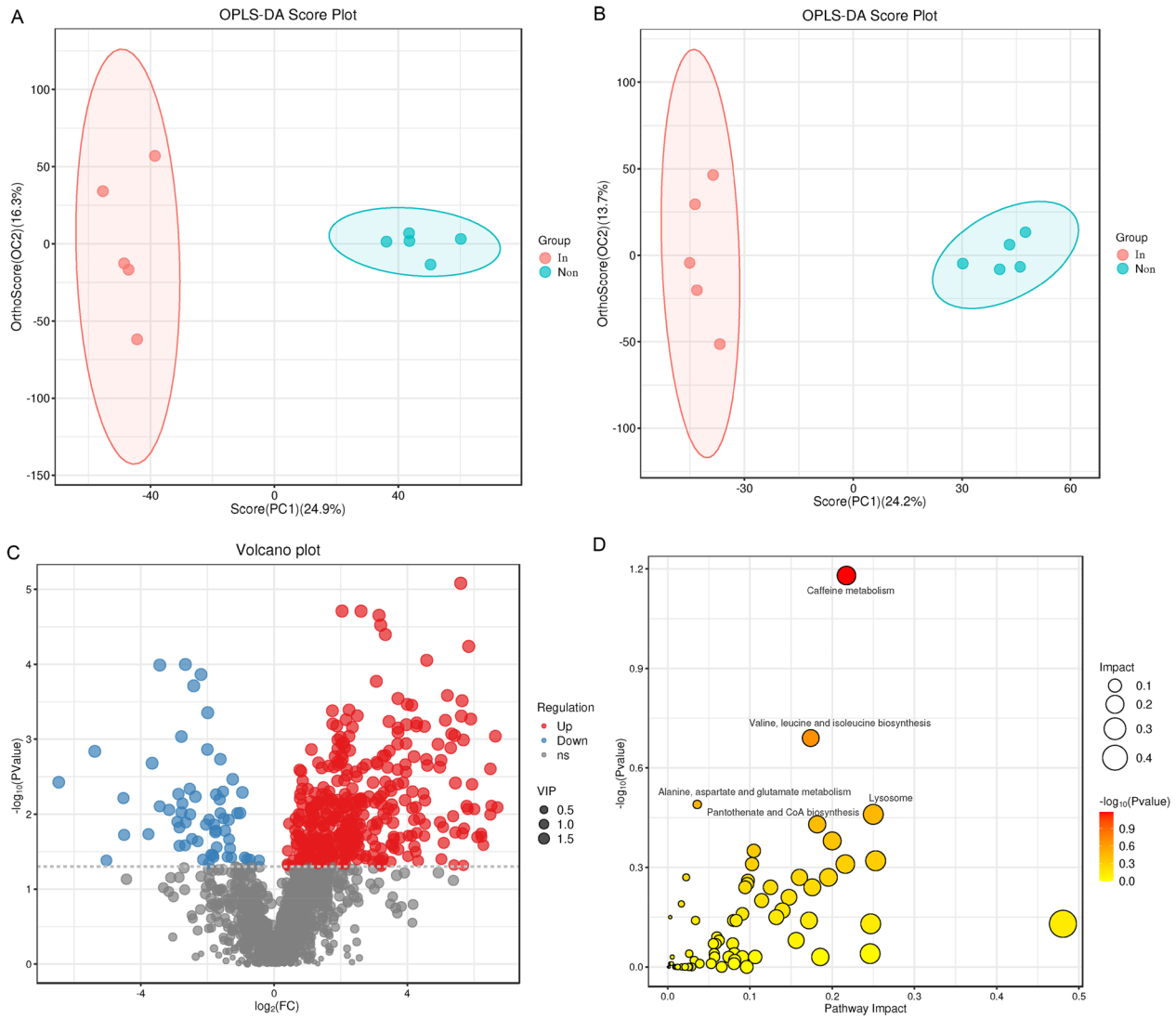

Figure 2 Metabolomic pattern variation in the heart tissues of Wenchang chickens infected with MDV. A OPLS-DA score plot of positive ions. **B** OPLS-DA score plot of negative ions. **C** Volcano plot of DEMs. **D** KEGG pathway enrichment of DEMs.

relationships, whereas values less than 0 represented negative associations. Gene–metabolite pairs with correlation coefficients > 0.8 and p values < 0.05 were classified as strongly correlated. The correlation heatmaps and interaction networks of the top 50 differentially abundant metabolites and genes are presented in Figures 3A and B (Additional file 7). These results demonstrated significant transcript–metabolite interactions. Both DEGs and DEMs were annotated against the KEGG pathway database, but no shared significantly enriched pathways were identified. To further investigate enzyme–metabolite regulatory relationships, DEGs and DEMs were mapped to the KEGG enzyme database. The top 10 associations ranked by $|\log_2\text{FoldChange}|$ magnitude are displayed in Figure 3C (Additional file 8). Among these, L-kynurenine paired with KYNU, KMO, KYAT3, and AADAT emerged as the most representative interaction.

Discussion

Previous studies have documented the global gene expression response to MDV infection in chickens [13, 15, 17, 18, 20–23, 40, 41]. Although these analyses provide valuable and important insights into host responses and virus–host interactions, their scope is limited by the coverage of the gene arrays used and the use of highly selected breeds/lines that show differential resistance to MDV challenges under laboratory conditions. In

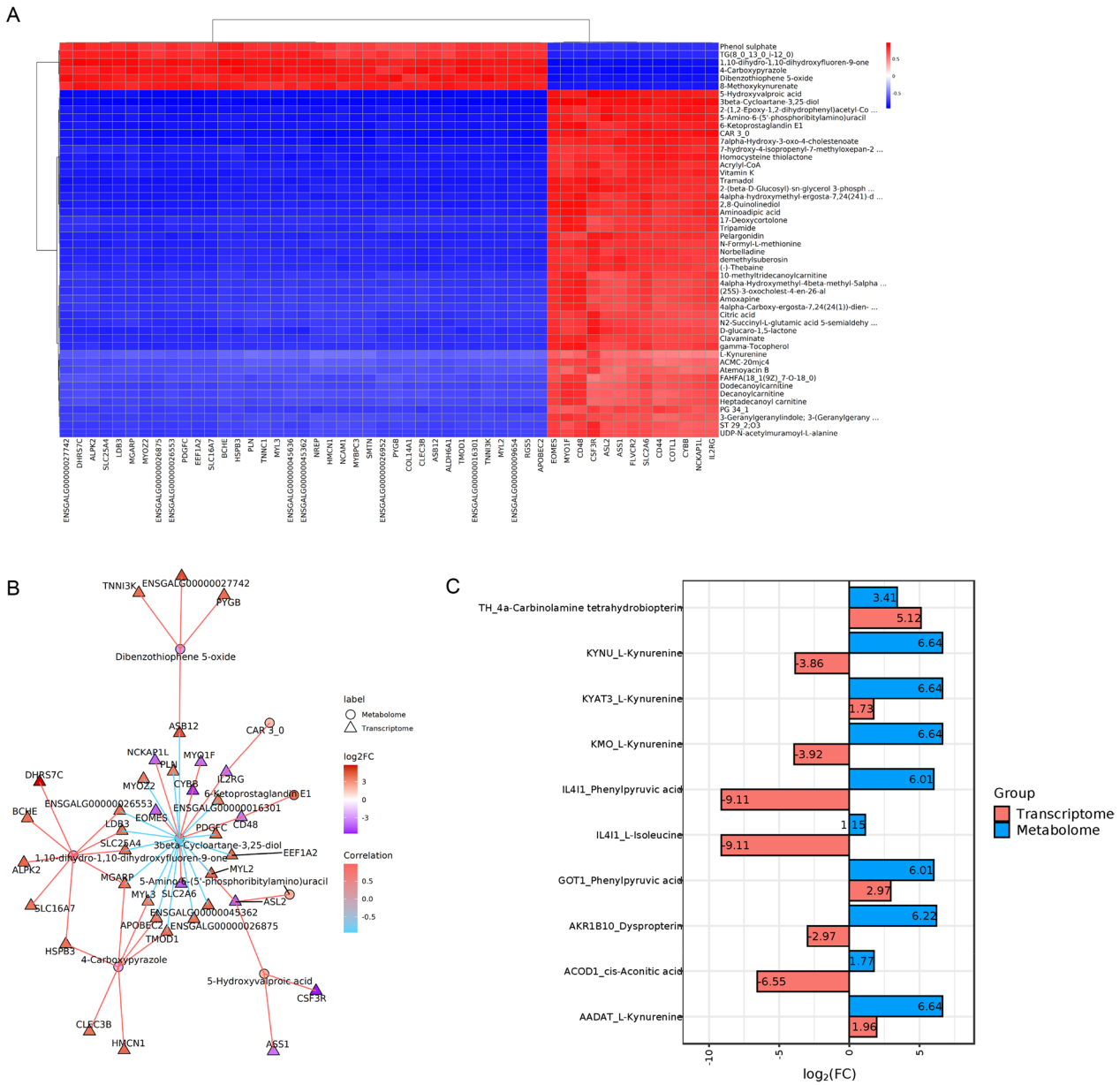

Figure 3 Comprehensive Analysis of Transcriptomics and Metabolomics. A Correlation heatmap of the top 50 significantly expressed genes and significantly expressed metabolites. **B** Correlation network of the top 50 significantly expressed genes and significantly expressed metabolites. **C** Top 10 corresponding relationships between metabolites in metabolic processes and the expression regulation of enzymes.

this study, we further expanded the current knowledge of host transcriptomic and metabolomic responses to MDV infection by comparing the transcriptome and metabolome changes in the Chinese native breed Wenchang chicken under natural conditions via RNA-seq and untargeted metabolomics technology. This study focused mainly on the tumor transformation stage after MDV infection. Our results revealed distinct transcriptomic and metabolomic patterns that may confer an immune response to MD.

Close examination of the transcriptomic changes in response to MDV infection revealed that immune-related genes (IRGs) were activated in infected Wenchang chickens. Compared with the list of 1546 IRGs downloaded

from the Gene Ontology Resource, the KEGG pathway database and DisGeNET, a total of 651 IRGs were significantly impacted by MDV infection in this study, including 459 upregulated and 192 downregulated genes (Additional file 9). Among these genes, many have been previously described in studies of the host response to MDV exposure [13, 15, 17, 18, 20–23, 40, 41], including genes related to chemokines (CCL19 and CXCL13L2), cytokines (IL21R, IL2RA), the innate immune response (IRF1, STAT1, CD36, IFIH1, SLC11A1, GCH1), and the adaptive immune response (B2M, P2RX7, SLC11A1). This overlap confirms that these candidate genes may play important roles in the response to MDV challenge. On the other hand, the six genes differentially expressed in this study (F13A1, HSP90AB1, RGS5, MMP7, IL4I1, and ADAMTS2) were promising top candidate genes conferring genetic resistance to MD [41]. In addition, certain genes impacted in this study have been implicated in MDV resistance/susceptibility in previous studies. These include CTLA4, CD72, TRANK1, SOCS1, TLR4, CD7, EDN1, IL1B, IFNG, CD79B, and PTPN3 [12, 41, 42].

A list of 1325 genes has been mapped to quantitative trait loci regions for chickens resistant to MDV [10, 12–14, 40, ChickenQTLdb]. A total of 263 DEGs in this study, accounting for 19.85% of the 1325 quantitative trait region genes, were identified on the basis of their locations within QTL regions and their expression patterns after MDV infection, including EOMES, FST, CSTA, C1S, CSTA, C1S, LAG3, CTNNA2, CD79B, TRANK1, SOCS1, TLR4, and CD7 [12, 41]. Notably, six members of the B7 family and cell adhesion molecules (CD274, PDCD1LG2, CD86, CD80, DMA and CD4) were significantly induced by infection, whereas eight genes involved in oxidative phosphorylation and the mitochondrial respiratory chain (UQCRFS1, UQCRC2, UQCRC1, ATP5G3, ATP5PF, NDUFB6, SUCLG1 and PRDX3) were significantly reduced in infected birds. The eight pathways significantly enriched by these 263 genes were related mainly to immunity, and cell adhesion molecules; glycine, serine and threonine metabolism; and the intestinal immune network for IgA production were the most representative pathways (Additional file 10). The 112 upregulated genes were significantly mapped into three pathways of the intestinal immune network for IgA production, cell adhesion molecules, and the Toll-like receptor signalling pathway, whereas the 151 downregulated genes were markedly enriched in eight pathways involved in metabolism, including glycine, serine and threonine metabolism; propanoate metabolism; glyoxylate and dicarboxylate metabolism; tryptophan metabolism; and pyruvate metabolism.

Many studies have revealed how MDV cleverly uses and reshapes the metabolic network of host cells to facilitate its own replication and assembly [27, 28, 43, 44]. In infected cells, viral replication relies heavily on the host machinery to produce large quantities of viral macromolecules and virus particles. The synthesis of the building blocks of viral particle-nucleotides, viral proteins, amino acids, lipid acids and genomes and the transport of viral components in the cell require energy, typically in the form of ATP. In addition to the downregulation of fatty acid metabolism, many downregulated genes were enriched in cellular respiration-related biological processes, such as cellular respiration, the respiratory electron transport chain, ATP synthesis coupled with electron transport, and mitochondrial respiratory chain complex assembly, in this study. Thus, many metabolic pathways, including valine, leucine and isoleucine degradation; glycine, serine and threonine metabolism; fatty acid degradation; the citrate cycle (TCA cycle); and pyruvate metabolism, were significantly enriched among the downregulated DEGs. Glycolysis is a major metabolic pathway in the cytoplasm that produces not only ATP but also metabolites for biosynthetic pathways such as the synthesis of lipids, amino acids, and nucleic acids. Pyruvate occupies a central metabolic node by virtue of its position at the crossroads of glycolysis and the tricarboxylic acid (TCA) cycle through the malic enzyme pathway to generate NADPH to support lipid biosynthesis. Pyruvate kinase catalyzes the final step of glycolysis, the production of pyruvate and ATP from glucose. In infected cells, glycolytic pyruvate kinase is directly recruited to the viral replicase complex to generate ATP for RNA synthesis [45]. Thus, we propose that the host may actively respond to MDV infection and tumor progression by regulating the balance between immunity and metabolism, which needs further investigation.

Mapping of differentially expressed genes and metabolites to the KEGG database revealed that L-kynurenine pairing with KYNU, KMO, KYAT3 and AADAT may function in host–virus interactions during MDV infection and tumor progression in cardiac tissue. Tryptophan is metabolized primarily through the kynurenine pathway, where it is converted to N-formyl-kynurenine by indoleamine-2,3-dioxygenase (IDO1 or IDO2) and tryptophan-2,3-dioxygenase (TDO2) and then demethylated to form kynurenine. Kynurenine is processed into either kynurenic acid or NAD + through two main branches of the kynurenine pathway. In the NAD + branch pathway, kynurenine is converted to NAD + via three different enzymes: kynurenine 3-monooxygenase (KMO), kynureninease (KYNU), and 3-hydroxyanthranilic acid dioxygenase (HAAO) [46]. Recent studies have shown that kynurenine, a potent immunomodulatory molecule, inhibits the proliferation

and activity of T cells and natural killer cells and promotes the differentiation of regulatory T cells [47–50]. Hyperactivation of the kynurenine pathway promotes cancer cell invasion, metastasis, and chemoresistance and is associated with poor prognosis in a variety of cancers [51–54]. KMO, which uses NADPH or NADH as a coenzyme, hydroxylates kynurenine to form 3-hydroxykynurenine (3HK) [55]. Studies have indicated that KMO and its product quinolinic acid have broad-spectrum antiviral effects [56], and KMO is overexpressed in the tissues of patients with triple-negative breast cancer [57], colorectal cancer [58], and liver cancer [59]. Elevated KMO expression alters the formation of 3-hydroxykynurenine and quinolinic acid and regulates immune responses and tumor tolerance, and high KMO expression is correlated with poor tumor prognosis [57–59]. KYNU, a key enzyme in the kynurenine pathway, catalyzes the formation of the metabolites anthranilic acid or 3-hydroxyanthranilic acid from kynurenine or 3-hydroxykynurenine. 3-Hydroxyphthalaminobenzoic acid is a modulator of the immune response and enhances apoptosis via iron or manganese ions in monocytes and macrophages under inflammatory conditions, triggering the death of activated T cells by depleting intracellular glutathione [60]. Moreover, 3-hydroxyanthranilic acid can inhibit dendritic cell maturation and T-cell activation [61]. Several studies have shown that KYNU expression is significantly associated with small cell lung cancer [62], triple-negative breast cancer subtypes [63], and cutaneous squamous cell carcinoma [64]. In this study, L-kynurenine abundance was significantly greater in the heart tissues of MDV-infected Wenchang chickens than in those of normal Wenchang chickens, whereas the expression of genes encoding two key enzymes related to kynurenine metabolism, KYNU and KMO, was significantly lower. It is speculated that the host downregulates the expression of the KYNU and KMO genes to enhance its immune response to MDV infection and its induced tumors. The specific mechanisms of action require further investigation.

Supplementary Information

The online version contains supplementary material available at https://doi.org/10.1186/s13567-025-01618-5.

Additional file 1. Sequences of Primers used for qPCR validation.

Additional file 2. Identification of Marek's disease virus infection.

Additional file 3. DEGs.

Additional file 4. KEGG analysis of DEGs.

Additional file 5. KEGG analysis of DEGs.

Additional file 6. KEGG pathways associated with DEMs.

Additional file 7. Top 50 DEMs and DEG correlations.

Additional file 8. Top 10 corresponding relationships of DEMs and DEGs.

Additional file 9. IRGs.

Additional file 10. DEGs within the QTLR for MD resistance.

Acknowledgements
We thank Dr Bin Lin from Hainan Coconut Village Quality Wenchang Chicken Breeding Co., Ltd., for kindly providing the experimental materials and facilitating the experiment.

Authors' contributions
XX arranged and performed the experiments. JZ conducted the statistical analyses. SH, YF, and DL performed the experiments. TS and LZ wrote the manuscript. LS and GH performed the statistical analyses. RZ supervised the study and modified the manuscript. GR designed the study and revised the manuscript. All authors read and approved the final manuscript.

Funding
This work was supported by the Chinese Academy of Tropical Agricultural Sciences for Science and Technology Innovation Team of the National Tropical Agricultural Science Center [CATASCXTD202407], the Key R & D Program of Hainan Province [ZDYF2021XDNY178, ZDYF2024KJTPY032], and the Wenchang Chicken Superiority Characteristic Industrial Cluster Project of Hainan Province, China [WCSCICP2023].

Availability of data and materials
The raw RNA-seq data are available in the National Genomics Data Center (NGDC) Genome Sequence Archive (GSA: CRA013443). The raw metabolomic datasets in the current study are available from the corresponding author upon reasonable request.

Declarations

Ethics approval and consent to participate
All procedures involving care and management were approved by the Institutional Animal Care and Use Committee of the Chinese Academy of Tropical Agricultural Sciences (Approval No. CATAS-20240520-2).

Competing interests
The authors declare that they have no competing interests.

Received: 18 March 2025 Accepted: 25 July 2025
Published online: 07 October 2025

References

1. Morrow C, Fehler F (2004) Marek's disease: A worldwide problem. In: Davison F, Nair V (eds) Marek's disease an evolving problem. Elsevier, pp 49–61
2. Baigent SJ, Davison F (2004) Marek's disease virus: biology and life cycle. In: Davison F, Nair V (eds) Marek's disease an evolving Problem. Elsevier, pp 62–ii
3. Jarosinski KW, Tischer BK, Trapp S, Osterrieder N (2006) Marek's disease virus: lytic replication, oncogenesis and control. Expert Rev Vaccines 5:761–772
4. Witter RL, Calnek BW, Buscaglia C, Gimeno IM, Schat KA (2005) Classification of Marek's disease viruses according to pathotype: philosophy and methodology. Avian Pathol 34:75–90
5. Witter RL (1997) Increased virulence of Marek's disease virus field isolates. Avian Dis 41:149–163
6. Witter RL, Gimeno IM, Reed WM, Bacon LD (1999) An acute form of transient paralysis induced by highly virulent strains of Marek's disease virus. Avian Dis 43:704–720
7. Calnek BW (2001) Pathogenesis of Marek's disease virus infection. Curr Top Microbiol Immunol 255:25–55
8. Vallejo RL, Bacon LD, Liu HC, Witter RL, Groenen MA, Hillel J, Cheng HH (1998) Genetic mapping of quantitative trait loci affecting susceptibility to Marek's disease virus induced tumors in F2 intercross chickens. Genetics 148:349–360

9. Yonash N, Bacon LD, Witter RL, Cheng HH (1999) High resolution mapping and identification of new quantitative trait loci (QTL) affecting susceptibility to Marek's disease. Anim Genet 30:126–135
10. Heifetz EM, Fulton JE, O'Sullivan NP, Arthur JA, Cheng H, Wang J, Soller M, Dekkers JCM (2009) Mapping QTL affecting resistance to Marek's disease in an F6 advanced intercross population of commercial layer chickens. BMC Genomics 10:20
11. Heifetz EM, Fulton JE, O'Sullivan NP, Arthur JA, Wang J, Dekkers JC, Soller M (2007) Mapping quantitative trait loci affecting susceptibility to Marek's disease virus in a backcross population of layer chickens. Genetics 177:2417–2431
12. Smith J, Lipkin E, Soller M, Fulton JE, Burt DW (2020) Mapping QTL associated with resistance to avian oncogenic Marek's disease virus (MDV) reveals major candidate genes and variants. Genes (Basel) 11:1019
13. Smith J, Sadeyen JR, Paton IR, Hocking PM, Salmon N, Fife M, Nair V, Burt DW, Kaiser P (2011) Systems analysis of immune responses in Marek's disease virus-infected chickens identifies a gene involved in susceptibility and highlights a possible novel pathogenicity mechanism. J Virol 85:11146–11158
14. Lipkin E, Smith J, Soller M, Burt DW, Fulton JE (2023) Sex differences in response to Marek's disease: mapping Quantitative Trait Loci Regions (QTLRs) to the Z chromosome. Genes (Basel) 14:20
15. Morgan RW, Sofer L, Anderson AS, Bernberg EL, Cui J, Burnside J (2001) Induction of host gene expression following infection of chicken embryo fibroblasts with oncogenic Marek's disease virus. J Virol 75:533–539
16. Karaca G, Anobile J, Downs D, Burnside J, Schmidt CJ (2004) Herpesvirus of turkeys: microarray analysis of host gene responses to infection. Virology 318:102–111
17. Sarson AJ, Abdul-Careem MF, Zhou H, Sharif S (2006) Transcriptional analysis of host responses to Marek's disease viral infection. Viral Immunol 19:747–758
18. Sarson AJ, Parvizi P, Lepp D, Quinton M, Sharif S (2008) Transcriptional analysis of host responses to Marek's disease virus infection in genetically resistant and susceptible chickens. Anim Genet 39:232–240
19. Kano R, Konnai S, Onuma M, Ohashi K (2009) Microarray analysis of host immune responses to Marek's disease virus infection in vaccinated chickens. J Vet Med Sci 71:603–610
20. Heidari M, Sarson AJ, Huebner M, Sharif S, Kireev D, Zhou H (2010) Marek's disease virus-induced immunosuppression: array analysis of chicken immune response gene expression profiling. Viral Immunol 23:309–319
21. Yu Y, Luo J, Mitra A, Chang S, Tian F, Zhang H, Yuan P, Zhou H, Song J (2011) Temporal transcriptome changes induced by MDV in marek's disease-resistant and-susceptible inbred chickens. BMC Genomics 12:501
22. Hu X, Qin A, Xu W, Wu G, Li D, Qian K, Shao H, Ye J (2015) Transcriptional analysis of host responses to Marek's disease virus infection in chicken thymus. Intervirology 58:95–105
23. Perumbakkam S, Muir WM, Black-Pyrkosz A, Okimoto R, Cheng HH (2013) Comparison and contrast of genes and biological pathways responding to Marek's disease virus infection using allele-specific expression and differential expression in broiler and layer chickens. BMC Genomics 14:64
24. Maceachern S, Muir WM, Crosby S, Cheng HH (2011) Genome-wide identification of allele-specific expression (ASE) in response to Marek's disease virus infection using next generation sequencing. BMC Proc 5(Suppl 4):S14
25. Chen C, Li H, Xie Q, Shang H, Ji J, Bai S, Cao Y, Ma Y, Bi Y (2011) Transcriptional profiling of host gene expression in chicken liver tissues infected with oncogenic Marek's disease virus. J Gen Virol 92:2724–2733
26. Djeraba A, Musset E, van Rooijen N, Quéré P (2002) Resistance and susceptibility to Marek's disease: nitric oxide synthase/arginase activity balance. Vet Microbiol 86:229–244
27. Boodhoo N, Kamble N, Sharif S, Behboudi S (2020) Glutaminolysis and glycolysis are essential for optimal replication of Marek's disease virus. J Virol 94:e01680
28. Wang Q, Shi B, Yang G, Zhu X, Shao H, Qian K, Ye J, Qin A (2003) Metabolomic profiling of Marek's disease virus infection in host cell based on untargeted LC-MS. Front Microbiol 14:1270762
29. Kim D, Langmead B, Salzberg SL (2015) Hisat: a fast spliced aligner with low memory requirements. Nat Methods 12:357–360
30. Putri GH, Anders S, Pyl PT, Pimanda JE, Zanini F (2020) Analysing high-throughput sequencing data in Python with HTSeq 2.0. Bioinformatics 38:2943–2945
31. Love MI, Huber W, Anders S (2014) Moderated estimation of fold change and dispersion for RNA-seq data with DESeq2. Genome Biol 15:550
32. Alexa A, Rahnenfuhrer J, Lengauer T (2006) Improved scoring of functional groups from gene expression data by decorrelating GO graph structure. Bioinformatics 22:1600–1607
33. Yu G, Wang LG, Han Y, He QY (2012) ClusterProfiler: an R package for comparing biological themes among gene clusters. OMICS 16:284–287
34. Zhou G, Soufan O, Ewald J, Hancock REW, Basu N, Xia J (2019) NetworkAnalyst 3.0: a visual analytics platform for comprehensive gene expression profiling and meta-analysis. Nucleic Acids Res 47:W234–W241
35. Zelena E, Dunn WB, Broadhurst D, Francis-McIntyre S, Carroll KM, Begley P, O'Hagan S, Knowles JD, Halsall A, HUSERMET Consortium, Wilson ID, Kell DB (2009) Development of a robust and repeatable UPLC-MS method for the long-term metabolomic study of human serum. Anal Chem 81:1357–1364
36. Want EJ, Masson P, Michopoulos F, Wilson ID, Theodoridis G, Plumb RS, Shockcor J, Loftus N, Holmes E, Nicholson JK (2013) Global metabolic profiling of animal and human tissues via UPLC-MS. Nat Protoc 8:17–32
37. Thévenot EA, Roux A, Xu Y, Ezan E, Junot C (2015) Analysis of the human adult urinary metabolome variations with age, body mass index, and gender by implementing a comprehensive workflow for univariate and OPLS statistical analyses. J Proteome Res 14:3322–3335
38. Xia J, Wishart DS (2011) Web-based inference of biological patterns, functions and pathways from metabolomic data using MetaboAnalyst. Nat Protoc 6:743–760
39. Csardi G, Nepusz T (2006) The igraph software package for complex network research. Interjournal Complex Syst 1695:1–9
40. Liu H, Cheng HH, Tirunagaru V, Sofer L, Burnside J (2001) A strategy to identify positional candidate genes conferring Marek's disease resistance by integrating DNA microarrays and genetic mapping. Anim Genet 32:351–359
41. Dong K, Chang S, Xie Q, Zhao P, Zhang H (2019) RNA sequencing revealed differentially expressed genes functionally associated with immunity and tumor suppression during latent phase infection of a vv + MDV in chickens. Sci Rep 9:14182
42. Chakraborty P, Kuo RI, Wu Z, Morris KM, Dutia BM, Kaiser P, Smith J (2022) The role of dendritic cells in the host response to Marek's disease virus (MDV) as shown by transcriptomic analysis of susceptible and resistant birds. Pathogens 11:1340
43. Heaton NS, Randall G (2010) Dengue virus-induced autophagy regulates lipid metabolism. Cell Host Microbe 8:422–432
44. Greseth MD, Traktman P (2014) De novo fatty acid biosynthesis contributes significantly to establishment of a bioenergetically favorable environment for vaccinia virus infection. PLoS Pathog 10:e1004021
45. Chuang C, Prasanth KR, Nagy PD (2017) The glycolytic pyruvate kinase is recruited directly into the viral replicase complex to generate ATP for RNA synthesis. Cell Host Microbe 22:639–652
46. Cristina B, Veronica R, Silvia A, Andrea G, Sara C, Luca P, Nicoletta B, Johanna MCB, Silvio B, Fabio T (2022) Identification and characterization of the kynurenine pathway in the pond snail *Lymnaea stagnalis*. Sci Rep 12:15617
47. Frumento G, Rotondo R, Tonetti M, Damonte G, Benatti U, Ferrara GB (2002) Tryptophan-derived catabolites are responsible for inhibition of T and natural killer cell proliferation induced by indoleamine 2,3-dioxygenase. J Exp Med 196:459–468
48. Terness P, Bauer TM, Röse L, Dufter C, Watzlik A, Simon H, Opelz G (2002) Inhibition of allogeneic T cell proliferation by indoleamine 2,3-dioxygenase-expressing dendritic cells: mediation of suppression by tryptophan metabolites. J Exp Med 196:447–457
49. Chiesa MD, Carlomagno S, Frumento G, Balsamo M, Cantoni C, Conte R, Moretta L, Moretta A, Vitale M (2006) The tryptophan catabolite l-kynurenine inhibits the surface expression of NKp46- and NKG2D-activating receptors and regulates NK-cell function. Blood 108:4118–4125
50. Yan Y, Zhang GX, Gran B, Fallarino F, Yu S, Li H, Cullimore ML, Rostami A, Xu H (2010) IDO upregulates regulatory T cells via tryptophan catabolite and suppresses encephalitogenic T cell responses in experimental autoimmune encephalomyelitis. J Immunol 185:5953–5961
51. de la Cruz GP, de la Cruz VP, Cossio JN, Cervantes GIV, Salazar A, Morales MO, Pineda B (2023) Kynureninase promotes immunosuppression and predicts survival in glioma patients: in silico data analyses of the Chinese

Glioma Genome Atlas (CGGA) and of the Cancer Genome Atlas (TCGA). Pharmaceuticals 16:369
52. Ye Z, Yue L, Shi J, Shao M, Wu T (2019) Role of IDO and TDO in cancers and related diseases and the therapeutic implications. J Cancer 10:2771–2782
53. Marin-Acevedo JA, Dholaria B, Soyano AE (2018) Next generation of immune checkpoint therapy in cancer: new developments and challenges. J Hematol Oncol 11:39
54. Burugu S, Dancsok AR, Nielsen TO (2018) Emerging targets in cancer immunotherapy. Semin Cancer Biol 52:39–52
55. Smith JR, Jamie JF, Guillemin GJ (2016) Kynurenine-3-monooxygenase: a review of structure, mechanism, and inhibitors. Drug Discov Today 21:315–324
56. Zhao J, Chen J, Wang C, Liu Y, Li M, Li Y, Li R, Han Z, Wang J, Chen L, Shu Y, Cheng G, Sun C (2022) Kynurenine-3-monooxygenase (KMO) broadly inhibits viral infections via triggering NMDAR/$Ca2^{+}$ influx and CaMKII/IRF3-mediated IFN-β production. PLoS Pathog 18:e1004021
57. Lai MH, Liao CH, Tsai NM, Chang KF, Liu CC, Chiu YH, Huang KC, Lin CS (2021) Surface expression of kynurenine 3-monooxygenase promotes proliferation and metastasis in triple-negative breast cancers. Cancer Control 28:10732748211009244
58. Liu CY, Huang TT, Chen JL, Chu PY, Lee CH, Lee HC, Lee YH, Chang YY, Yang SH, Jiang JK, Chen WS, Chao Y, Teng HW (2021) Significance of kynurenine 3-monooxygenase expression in colorectal cancer. Front Oncol 11:620361
59. Jin H, Zhang Y, You H, Tao X, Wang C, Jin G, Wang N, Ruan H, Gu D, Huo X, Cong W, Qin W (2015) Prognostic significance of kynurenine 3-monooxygenase and effects on proliferation, migration and invasion of human hepatocellular carcinoma. Sci Rep 5:10466
60. Lee SM, Lee YS, Choi JH, Park SG, Choi W, Joo YD, Lee WS, Lee JN, Choi I, Seo SK (2010) Tryptophan metabolite 3-hydroxyanthranilic acid selectively induces activated T cell death via intracellular GSH depletion. Immunol Lett 132:53–60
61. Lee WS, Lee SM, Kim MK, Park SG, Choi IW, Choi I, Joo YD, Park SJ, Kang SW, Seo SK (2013) The tryptophan metabolite 3-hydroxyanthranilic acid suppresses T cell responses by inhibiting dendritic cell activation. Int Immunopharmacol 17:721–726
62. Fahrmann JF, Tanaka I, Irajizad E, Mao X, Dennison JB, Murage E, Casabar J, Mayo J, Peng Q, Celiktas M, Vykoukal JV, Park S, Taguchi A, Delgado O, Tripathi SC, Katayama H, Soto LMS, Rodriguez-Canales J, Behrens C, Wistuba I, Hanash S, Ostrin EJ (2022) Mutational activation of the NRF2 pathway upregulates kynureninase resulting in tumor immunosuppression and poor outcome in lung adenocarcinoma. Cancers (Basel) 14:2543
63. Heng B, Bilgin AA, Lovejoy DB, Tan VX, Milioli HH, Gluch L, Bustamante S, Sabaretnam T, Moscato P, Lim CK, Guillemin GJ (2020) Differential kynurenine pathway metabolism in highly metastatic aggressive breast cancer subtypes: beyond IDO1-induced immunosuppression. Breast Cancer Res 22:113
64. Ci C, Wu C, Lyu D, Chang X, He C, Liu W, Chen L, Ding W (2020) Down-regulation of kynureninase restrains cutaneous squamous cell carcinoma proliferation and represses the PI3K/AKT pathway. Clin Exp Dermatol 45:194–201

Publisher's Note

Springer Nature remains neutral with regard to jurisdictional claims in published maps and institutional affiliations.